Dynamical and thermal effects of nonsteady nonlinear acoustic–gravity waves propagating from tropospheric sources to…

Article *in* Advances in Space Research · February 2015

DOI: 10.1016/j.asr.2015.01.033

CITATIONS
4

READS
62

2 authors:

Nikolai M. Gavrilov
Saint Petersburg State University
223 PUBLICATIONS **1,082** CITATIONS
SEE PROFILE

Sergey Kshevetskii
Immanuel Kant Baltic Federal University
71 PUBLICATIONS **180** CITATIONS
SEE PROFILE

Manuscript of the paper submitted to the journal.

Edited version of the paper is published in the journal "Advances in Space Research", 2015, v. 55, doi:10.1016/j.asr.2015.01.033

Dynamical and thermal effects of nonsteady nonlinear acoustic-gravity waves propagating from tropospheric sources to the upper atmosphere.

Nikolai M. Gavrilov[a], Sergey P. Kshevetskii[b],

[a]Atmospheric Physics Department, Saint-Peterburg State University, Saint-Peterburg, Russia
[b]Theoretical Physics Department, Immanuel Kant Baltic Federal University, Kaliningrad, Russia

(Received, 2014; Revised …, 2014; Accepted 2015; Online published Feb 2015)

Correspondence to Nikolai M. Gavrilov n.gavrilov@spbu.ru Sergey P. Kshevetskii renger@mail.ru

We performed numerical simulations of nonlinear AGW propagation to the middle and upper atmosphere from a plane wave forcing at the Earth's surface with period $\tau = 2\times10^3$ s. After activating the surface wave forcing, initial pulse of acoustic and very long gravity modes in a few minutes can reach altitudes above 100 km. Dissipation of this initial pulse produces substantial mean heating and wave-induced mean winds at altitudes above 200 km. This may influence AGW propagation and produce enhanced vertical gradients of temperature, horizontal velocity and increased wave dissipation in the lower part of the wave-induced mean flows helping their downward expansions. Later, AGWs may produce layers of convective instability and peaks of the wave-induced jets at altitudes 100 – 120 km. Shorter AGWs with smaller horizontal wave speeds produce smaller mean heating and wave-induced mean velocities in the upper atmosphere at fixed amplitudes and periods of the surface wave excitation. Numerical simulation of nonlinear AGW propagation helps better understanding the details of dynamical and thermal influence of waves coming from the troposphere on the mean temperature and wind in the middle and upper atmosphere.

Key words: Atmosphere; acoustic-gravity waves; nonlinear interactions; numerical modeling; wave drag

1. Introduction.

Observations show the continuous presence of GWs in the middle atmosphere (Fritts and Alexander, 2003, and the references therein). Increasing amount of observations suggest that GW can be frequently detected in the thermosphere (Djuth et al., 2004; Park et al., 2014). Recent general circulation modeling studies have demonstrated that lower atmospheric GWs can propagate into the thermosphere and produce appreciable dynamical (Yiğit et al., 2009) and thermal effects (Yiğit and Medvedev, 2009). Propagation and the resulting effects of small-scale GWs in the thermosphere exhibit significant variations during sudden stratospheric warmings (Yiğit and Medvedev, 2012a; Yiğit et al., 2014). A comprehensive review of internal gravity

wave propagation into the thermosphere and their effects was made by Yiğit and Medvedev (2014).

Non-hydrostatic numerical models are useful for AGW and turbulence studies. For example, Baker and Schubert (2000) performed modeling nonlinear AGWs in the Venus' atmosphere. They simulated waves in an atmospheric region with vertical and horizontal dimensions of 48 and 120 km, respectively. Other authors (Fritts and Garten, 1996; Andreassen et al., 1998; Fritts et al., 2009, 2011; Liu et al., 2009) made two-dimension modeling Kelvin-Helmholtz instabilities and turbulence generated due to breaking of atmospheric waves. These studies used three-dimensional models treating waves and turbulence in atmospheric boxes with limited horizontal and vertical sizes. The models used modifications of the spectral method and Galerkin-type series to convert partial (versus time) differential equations into the ordinary ones describing the spectral series coefficients. Liu et al. (2009) simulated gravity wave propagating from the lower atmosphere and generating Kelvin-Helmholtz billows in the mesopause region. Yu and Hickey (2007) and Liu et al. (2008) have developed two-dimensional numerical models of atmospheric AGWs.

In addition to direct numerical modeling, mesoscale AGWs generating in the troposphere and propagating to the thermosphere were studied in general circulation models (e.g., Yiğit et al., 2009, 2012a) using parameterizations of wave dynamical and thermal effects to describe their saturation and dissipation in the middle and upper atmosphere (e.g., Yiğit et al., 2008). These AGWs propagate upwards, break and produce turbulence and perturbations in the middle and upper atmosphere. For example, convection and mesoscale turbulence in the troposphere may produce AGWs (e.g., Fritts and Alexander , 2003; Fritts et al., 2006). Turbulent sources may have maxima at altitudes 9–12 km in the regions of tropospheric jet streams (Medvedev and Gavrilov, 1995; Gavrilov and Fukao, 1999; Gavrilov, 2007).). Using a nonhydrostatic general circulation model of the thermosphere-ionosphere system, Yiğit et al. (2012b) have demonstrated that gravity waves and acoustic waves are continuously present in the thermosphere even during quiet geomagnetic periods.

Gavrilov and Kshevtskii (2013a) modeled two-dimensional nonlinear AGWs using a numerical scheme accounting for the fundamental conservation laws. This scheme described in more detail by Kshevetskii and Gavrilov (2005) provides the necessary numerical stability and has allowed us to take into account non-smooth solutions of AGW nonlinear equations. Gavrilov and Kshevetskii (2013b, 2014a) made a three-dimension modification of this algorithm for modeling nonlinear atmospheric AGWs. They simulated AGWs generated by sinusoidal horizontally homogeneous wave forcing at the Earth's surface.

Karpov and Kshevetskii (2014) applied similar three-dimensional numerical model to simulate acoustic wave propagation from localized non-stationary surface wave excitation and found that infrasound could produce substantial mean heating in the thermosphere. Nonlinear dissipating AGWs are also responsible for creating accelerations of the mean flows (e.g., Fritts and Alexander, 2003). At the same time, details of the mean flows and heating produced by nonlinear non-stationary AGWs in the atmosphere need further clarifications.

In this paper, using the numerical model by Gavrilov and Kshevetskii (2013b, 2014a), we continue studying propagation of nonlinear AGWs generated at the Earth's surface into the thermosphere. We considered simple AGW forcing by plane wave oscillations of vertical velocity at the surface and considered details of wave dynamical and thermal effects at different altitudes at different times after activating the wave source. Compared to Karpov and Kshevetskii (2014) we considered lower frequencies of wave sources belonging to gravity wave subrange of AGW spectrum.

2. **Numerical model.**

The numerical AGW model simulates velocity components u, v, and w along horizontal (x, y) and vertical, z, axes, respectively. The model also calculates deviations of density ρ',

temperature T', and pressure p' from stationary background fields ρ_0, T_0 and p_0, respectively. One can find the used set of nonlinear hydrodynamic equations in the papers by Gavrilov and Kshevetskii (2013b, 2014a). The set includes equations of continuity, motion and heat balance. The conditions at upper boundary z = 500 km include zero vertical gradients of perturbations of pressure, temperature, density and horizontal velocity as well as zero vertical velocity. The lower boundary conditions at the Earth's surface include zero deviations of pressure, density, temperature and horizontal velocity (see Gavrilov and Kshevetskii, 2013a, b; 2014a).

In the present research, we suppose horizontal periodicity of wave solutions:

$$f(x,y,z,t) = f(x+L_x, y+L_y, z, t), \tag{1}$$

where f could be any of the calculated variables, and $L_x = m\lambda_x$, $L_y = n\lambda_y$ are the horizontal lengths of the considered region of the atmosphere, m and n are integer constants, λ_x and λ_y are wavelengths along horizontal axes x and y, respectively. Oscillations of vertical velocity $w_0 = w(x,y)$ at the earth's surface $z = 0$ force AGWs in the model.

Used numerical scheme is the generalization of two-dimensional algorithm developed by Kshevetskii and Gavrilov (2005) to the three-dimensional situation. Hydrodynamic equations of the model (see Gavrilov and Kshevetskii, 2013b, 2014a) may be written in the form of conservation laws

$$\frac{\partial r}{\partial t} + \frac{\partial X(r)}{\partial x} + \frac{\partial Y(r)}{\partial y} + \frac{\partial Z(r)}{\partial z} = 0, \tag{2}$$

where r denotes any of density, momentum or energy per unit volume, X, Y, Z are components of fluxes of respective quantities along axes x, y, z. We take into account terms containing gravity in the equation for vertical momentum component. In addition to the numerical scheme by Kshevetskii and Gavrilov (2005) the present thermal balance equation includes terms representing heating due to viscosity. Our numerical method uses the Lax and Wendroff (1960) scheme having the second order of accuracy, in which the finite-difference approximation of Eq. (2) has the following form:

$$\frac{r_{i,j,k}^{n+1} - r_{i,j,k}^{n}}{\Delta t} + \frac{X_{i+1/2,j,k}^{n+1/2} - X_{i-1/2,j,k}^{n+1/2}}{\Delta x} + \frac{Y_{i,j+1/2,k}^{n+1/2} - Y_{i,j-1/2,k}^{n+1/2}}{\Delta y} + \frac{Z_{i.j.k+1/2}^{n+1/2} - Z_{i,j,k-1/2}^{n+1/2}}{\Delta z} = 0, \tag{3}$$

where indices n, i, j, k and Δt, Δx, Δy, Δz, are numbers of grid nodes and grid spacing in t, x, y, z, respectively. This scheme allows us picking up generalized physically acceptable solutions of the equations (Lax, 1957; Richtmayer and Morton, 1967). It provides the stability of numerical method and let us taking into account non-smooth solutions of AGW nonlinear equations. We use a staggered grid, where density, temperature and pressure are given at the same mesh points, but nodes for the components of velocity u, v, w are shifted half grid spacing along axes x, y, z, respectively. To calculate $r^{n+1/2}$ at the first half step in time we use the implicit scheme

$$2\frac{r_{i,j,k}^{n+1/2} - r_{i,j,k}^{n}}{\Delta t} + \frac{X_{i+1/2,j,k}^{n+1/2} - X_{i-1/2,j,k}^{n+1/2}}{\Delta x} + \frac{Y_{i,j+1/2,k}^{n+1/2} - Y_{i,j-1/2,k}^{n+1/2}}{\Delta y} + \frac{Z_{i.j.k+1/2}^{n+1/2} - Z_{i,j,k-1/2}^{n+1/2}}{\Delta z} = 0, \tag{4}$$

This significantly complicates computations; however, Kshevetskii (2001a, b, c) had shown that the errors from acoustic waves are not accumulated with time for finite-difference schemes of such a structure.

Our numerical model includes molecular viscosity and heat conductivity increasing with altitude inversely proportional to density. Balloon, rocket and satellite measurements (e.g., Lubken, 1996; Clayson and Kantha, 2008) show intensive background turbulence in the

boundary layer and in the lower thermosphere with very weak turbulence in the stratosphere (e.g., Gavrilov et al., 2005, 2013). In the model, we take into account background turbulent specific viscosity and heat conductivity approximating their vertical profiles with the sum of two generalized bell-shaped functions (MathWorks, 2014) having maxima 10 m^2/s at altitudes 0 and 100 km with half widths of 1 km and 20 km, respectively. The model does not involve some effects, for example, wave dissipation due to radiative heat exchange and ion drag. However, dissipation due to ion drag can compete with molecular viscosity in the lower thermosphere at high solar activity and ionization (e.g., Yiğit et al., 2008).

In the present paper, we use background vertical profiles of ρ_0, T_0, and p_0 from the standard atmosphere model MSIS-90 (Hedin, 1991) for January and average geomagnetic activity. The average spacing of vertical grid is about 170 m, but it is smaller in the lower boundary layer and is changing with height depending on inhomogeneity of temperature profiles, varying from 12 m near the ground to about 1.2 km at altitudes about 500 km. Spacing of the horizontal grid in the present study is 1/60 of horizontal wavelengths specified in the wave forcing (5). Time steps are calculated automatically to assure stability of the numerical scheme and are equal to 0.14 s and 0.24 s for considered here AGWs with c_h = 30 m/s and c_h = 100 m/s, respectively.

In the present paper, we analyze such characteristics as the mean velocity and the wave accelerations of the mean flow. The mean values are calculated for each altitude and time instance by averaging over horizontal regions containing integer number of AGW periods vs. horizontal axes. Influence of waves on the mean flow are determined by horizontal components of wave drag $a_{wi} = -\rho_0^{-1} \partial \rho_0 \langle v_i' w' \rangle / \partial z$, where v_i is the component velocity along the i-th horizontal axis and the sign <> denotes averaging over wave periods. To obtain them, we calculated values $v_i' w'$ in every grid point and averaged them over horizontal planes at each altitude.

3. Results of simulations.

Gavrilov and Kshevetskii (2013a, b) simulated nonlinear AGWs having forms of plane waves. In the present study, we also assume horizontally periodical distributions of vertical velocity at the Earth's surface of the form of

$$(w)_{z=0} = W_0 \cos[k_h(x - c_h t)], \qquad (5)$$

where $k_h = 2\pi/\lambda_h$ and c_h are wavenumber and phase speed along the horizontal axis x directed in the wave propagation direction; W_0 is amplitude. Eq. (5) represents plane wave of vertical velocity at the lower boundary. This forcing may represent spectral components of turbulent and convective AGW sources (Townsend, 1965, 1966). In the present study, we made simulations for c_h between 10 and 100 m/s. The numerical modeling was made starting from zero initial conditions at t = 0, when the wave forcing at the bottom boundary was activating.

Medvedev and Gavrilov (1995) considered AGW generation due to nonlinear interactions produced by turbulent and meteorological processes in the atmosphere. They found broad variety of amplitudes, wavelengths and other parameters of generated AGWs. Gavrilov and Kshevetskii (2013a, b; 2014a) showed that activating the plane wave forcing at the bottom boundary initiates pulses of acoustic and very long gravity waves propagating upwards. Figure 1 shows examples of vertical profiles of temperature perturbations at fixed horizontal coordinates at different times t after activation of the surface AGW excitation (5) with horizontal phase speed c_h = 100 ms^{-1}. After activating the surface wave source, acoustic and very long gravity wave components will quickly propagate to high altitudes.

Figure 1 represents individual vertical profiles for fixed horizontal coordinate x. Figures 1 a – c show that in the plane wave approximation (5), initial wave pulses in a few minutes can reach altitudes of 100 km and above and form quasi-vertical wave fronts similar to those shown in

Figure 1 of the paper by Gavrilov and Kshevetskii (2013a). At high altitudes, these first wave pulses strongly dissipate because of molecular viscosity and heat conduction. As time increases, larger vertical wavelength waves are progressively removed by dissipation and vertical wavelengths should decrease with increasing time at fixed altitudes in the middle atmosphere (Vadas and Fritts, 2005; Vadas and Nicolls, 2012; Liu et al., 2013; Heale et al., 2013). This may explain the decrease in vertical wavelengths in Figures 1 f,g compared to Figures 1 b,c. After some transition period, primary acoustic and long gravity wave modes disperse and dissipate, then the vertical profiles in Figures 1 e, f correspond to the main spectral component of the wave source (5) with horizontal wave number k_h and horizontal phase speed c_h.

Respective profiles at other horizontal distances x are different from Figure 1due to changes in AGW phases. These profiles for all x at fixed times t are plotted in Figure 2. The profiles are superimposed. Therefore, Figure 2 allows seeing only ranges of temperature perturbations produced by waves at different altitudes. These perturbations include periodical wave variations and changes in the background mean profiles calculated as average values for each altitude and shown with thick solid lines in Figure 2. In Figure 2b, one can observe changes in the mean temperature at altitudes 200 – 400 km just 0.2 h after the wave forcing activation. Figure 2c reveals substantial increase in the mean temperature above 250 km due to dissipation of the initial acoustic pulse caused by strong molecular viscosity and heat conduction at high altitudes. The acoustic nature of this pulse can be confirmed by its high vertical group velocity (about 295 m/s to reach altitude of 350 km in 0.33 hr in Figure 2c).

Time of propagation of AGW energy from the Earth's surface to altitude z can be estimated as $t_e \sim z\tau/\lambda_z$, where τ and λ_z are the wave period and average vertical wavelength, respectively. For considered main wave component of the wave excitation (5) with λ_h = 200 km and c_h = 100 m/s from the standard AGW theory (e.g. Gossard and Hook, 1975), we have estimates $\tau = 2\times10^3$ s, $\lambda_z \sim 30$ km and $t_e \sim (3.3 – 6.6)\tau \sim 2$ - 4 hr for altitudes 100 – 200 km. Considerations of Figures 2e,f for later times reveal smaller (than that in Figure 2c) changes in the mean temperature above 200 km and some its increases at altitudes near 100 km.

Figure 3 is similar to Figure 2, but represents ranges of horizontal velocity perturbations at different times t produced by the same AGW surface excitation. Figure 3a shows appearance of the wave-induced mean jet stream at altitudes 200 – 250 km at t = 1 hr. This time is smaller than above estimated time t_e of arrival of the main gravity wave mode of the wave source (5) to altitudes 200 – 250 km. Therefore, the reason for wave induced jet stream in Figure 3a should be dissipation of initial acoustic-gravity wave pulse generated after activation of the wave source. In Figures 3b,c one can see that the wave induced jet stream become stronger in time and its maximum shifts downwards. At t > 4 hr, after arriving the main gravity mode to altitudes above 100 km, the peaks of wave-induced jets in Figures 3d-e tend to concentrate at altitudes 110 – 120 km with largest growing in the mean horizontal velocity near 100 km.

Figures 4b and 4c present, respectively, the ranges of vertical gradients of horizontal velocity and temperature during the mean heating in the upper atmosphere at t = 0.33 – 0.5 hr (see Figure 2c). These gradients include contributions from vertical inhomogeneities of the background fields and wave perturbations. In Figure 4b, one can see that the regions of maximum mean heating at altitudes above 200 km correspond to maximum vertical gradients of horizontal velocity during passage of the initial AGW pulses. Vertical temperature gradients in Figure 4c are mainly due to inhomogeneities of the background MSIS temperature profile.

Figures 5b and 5c represent vertical gradients of horizontal velocity and temperature similar to Figures 4b,c, but for later t ~ 1.8 – 3 hr, when the wave induced jet stream shown in Figure 5a already exists in the upper atmosphere. Increase in the mean horizontal velocity in Figure 5a above altitude 150 km change intrinsic frequency of AGWs propagating from below. This form larger gradients and their variability in Figures 5b,c at altitudes near and below the maximum of the jet stream in Figure 5a. Higher gradients lead to increased AGW dissipation by molecular viscosity and heat conduction and to further acceleration of the mean flow by waves. Such self-

accelerated process leads to expansion of the region of high mean velocities downwards (see Figure 3).

The top panel of Figure 5c shows that during passage of initial AGW pulse always dT/dz > - γ_a (where $\gamma_a = g/c_p$ is adiabatic temperature gradient, c_p is the specific heat capacity at constant pressure), which means convective stability of the atmosphere. After t ~ 2 – 3 hr, when the energy of the main gravity mode reach altitudes about 100 km, the layers with dT/dz < - γ_a appear in the bottom panel of Figure 5c. These regions correspond to convective instabilities of wave profiles and generation of turbulence increasing dissipation and wave drag (Lindzen, 1981). This increase and stabilize the maximum of wave induced jet stream at altitudes just above 100 km as shown in Figures 3d-f.

Figure 6 presents time variations of the wave-induced mean horizontal velocities at different fixed altitudes in the upper and middle atmosphere. Above 110 km, strong wave-induced jet stream appears first at higher altitudes and then propagates downwards in accordance with Figures 3 and 5. As time increases, the speeds of wave-induced mean velocity tend to a maximum values close to the wave horizontal phase speed c_h in Figures 6b and 6d corresponding to altitudes 110 and 150 km, respectively. Below 100 km, Figures 6d and 6e also show increases in the wave-induced mean horizontal velocity caused by molecular and turbulent AGW dissipation, but values of these velocities are much smaller, than that at higher altitudes in Figures 6a-c.

Time variations of the mean temperature changes produced by the wave forcing (5) with c_h = 100 m/s at different altitudes are shown in Figure 7. At altitudes 110 – 250 km largest increases in the mean temperature in Figures 7 a-c occur at $t \sim (3 – 5)\tau$. Below 100 km the temperature increases are smaller and temperature even decreases in time in Figures 7 d,e. Our model involves heating rates caused by molecular viscosity and heat conduction. The latter may produce heating or cooling the atmosphere depending on the shape of the vertical profile of the background temperature. Used in our calculations MSISE temperature profile for January (see Figure 1 in Gavrilov and Kshevetskii, 2014a) corresponds to heat conduction cooling of the atmosphere at altitudes of 60 and near 100 km. Therefore, when heating produced by dissipation of wave energy decreases because of the wave energy transfer to the mean flow shown in Figures 6c,d, the influence of the heat conduction cooling becomes noticeable in Figures 7 c,d. At altitude 60 km, the dissipation of wave energy is always small and we see permanent decrease in the mean temperature in Figure 7e.

Wave-induced increases in the thermospheric temperature seen in Figures 2 and 7 confirm previous results about AGW substantial contribution to the thermal regime of the upper atmosphere. For example, Yiğit and Medvedev (2009) have shown that GWs can produce significant thermal effects (heating) in the lower thermosphere. Additionally, Yiğit and Medvedev (2010) have shown that GW thermal effects exhibit large variations with the solar activity.

Figure 8 displays horizontal wave accelerations of the mean flow, a_{wh}, produced by the wave source (5) with c_h = 100 m/s. At altitudes above 110 km in Figures 8 a-c, a_{wh} are mainly positive and maximized at times of faster growing the mean wind at respective altitudes shown in Figures 6 a-c. Peak values of the wave accelerations an altitudes 110 – 250 km may reach $(2\text{-}3)\times10^3$ m/s/day, which provide very fast growing the mean wind in Figures 6a-c. Below 100 km, in Figures 8d,e AGW dissipation and a_{wh} magnitudes become smaller and the proportion of negative a_{wh} values increases. This assumes an increase in the number of downward propagating wave pulses reflected and generated in the atmosphere at higher altitudes. Such partial reflection of AGW modes and their interferences with the upward propagating main wave may explain higher variability of characteristics shown at lower panels of Figures 6 – 8.

All the above results are obtained for the wave excitation (5) with horizontal phase speed c_h = 100 m/s, which has relatively large vertical wavelength and can propagate up to very high altitudes. We also made calculations for smaller c_h = 30 m/s. Respective wave-induced mean horizontal velocities and temperatures at different altitudes are given in Figures 9 and 10.

Smaller c_h corresponds to smaller $\lambda_z \sim 10$ km and larger time of energy propagation of the main mode of wave excitation (5) to altitudes 100 – 200 km $t_e \sim (10 – 20)\tau \sim 6$ - 12 hr. Therefore, changes in the wave-induced mean wind at high altitudes in Figure 9 occur later than that in Figure 6. In addition, maximum mean velocity in Figure 9c is smaller than that in Figure 6c. This corresponds to expectations that at $t \to \infty$ the velocity of the wave-induced mean flow should tend to c_h and is larger for larger wave horizontal phase speed. Shorter vertical wavelength mode with $c_h = 30$ m/s is subject for stronger dissipation due to molecular and background turbulent viscosity and heat conduction in the middle and upper atmosphere. Therefore, magnitudes of wave-induced mean flows at altitudes 200 – 250 km for $c_h = 30$ m/s are much smaller in Figures 9a,b, than those in Figures 6a,b for $c_h = 100$ m/s. The mean temperature increases for $c_h = 30$ m/s in Figures 9a,b at altitudes 150 – 250 km exist during dissipation of initial AGW pulses only and are several times smaller than those for $c_h = 100$ m/s in Figures 7a,b.

Larsen (2000) and Larsen et al. (2005) found frequent intensive jet streams at altitudes near 100 km. Several explanations exist for the reasons of these jets, such as statistic stability requirement (Liu, 2007), semi-diurnal tidal modulations (Yue et al., 2010), nonlinear interactions among gravity waves, mean flow, and tide (Liu et al., 2014a, 2014b). Considered in Figures 3d-f grows in the mean flow superimposed on the AGW variations may be one of the mechanisms of creation of strong narrow peaks of horizontal velocity in the upper atmosphere. Figure 6 reveals that intervals of only few wave periods could be sufficient for formation of such peaks even at moderate amplitudes of the wave forcing in the numerical model.

Figure 5 shows quite long transition time intervals of getting developed structures of stationary AGWs after activating the lower boundary wave excitation (5). Average characteristics of the wave fields change during these transition intervals. Observations (e.g., Fritts and Alexander, 2003) frequently reveal relatively short pulses of a few AGW wavelengths and periods in the atmosphere. This shows that working times of many AGW sources in the atmosphere are relatively short (e.g., Fritts et al., 2006). Respective AGW pulses may have not enough time for becoming stationary during the activity of the wave sources. Therefore, we may assume that a substantial proportion of AGWs observed in the atmosphere may be non-stationary.

Karpov and Kshevetskii (2014) used another version of the same numerical model and considered propagation of infrasonic waves from localized surface excitation. They found substantial mean heating similar to our Figures 2c and 7a at altitudes 200 – 300 km. Results of the present study for longer period wave sources involving gravity wave modes show that heat effects dominate in the thermosphere during first transition interval, when initial acoustic wave pulses dissipate at high altitudes. Later, when the energy of gravity wave modes propagates to high altitudes, prevailing become dynamical wave effects leading to wave-induced mean flows in the middle and upper atmosphere.

For infrasound wave source, thermospheric wave heating lasts longer and can span horizontal regions with dimensions up to thousand km (Karpov and Kshevetskii, 2014). Therefore, local wave sources can produce large-scale inhomogeneities in temperature and horizontal winds in the upper atmosphere. These inhomogeneities, in turn, may modify conditions of AGW propagation (e.g., Karpov and Kshevetskii, 2014). We need additional observations and modeling for better knowledge of perturbations and modifications of the mean temperature and winds produced by variable AGW sources in the atmosphere.

Direct numerical AGW simulations performed in this study may be useful for verifications of simple parameterizations of wave dynamical and thermal effects for atmospheric general circulation models. Such parameterizations usually use simplified linear AGW theories and relations. Therefore, comparisons of numerically modeled and simplified analytical relations may be essential for obtaining scope of feasibility of analytical relations and for testing of AGW parameterizations (e.g., Gavrilov and Kshevetskii, 2014b).

Conclusion

We performed numerical simulations of nonlinear AGW propagation to the middle and upper atmosphere from a plane wave forcing at the Earth's surface with period $\tau = 2\times10^3$ s. After activating the surface wave forcing at $t = 0$, initial pulse of acoustic and very long gravity modes in a few minutes can reach high altitudes above 100 km. Dissipation of this initial pulse by strong molecular viscosity and heat conduction produces substantial increases in the mean temperature and horizontal wind at altitudes above 200 km. These initial mean heating and wave-induced jet stream increase Brunt-Vaisala frequency, decrease intrinsic frequency and influence AGW propagation producing larger vertical gradients of temperature and horizontal velocity in the lower part of the wave-induced mean flow, which increase dissipation and wave drag. This causes the downward expansion of the wave-induced jet stream. After arriving the energy of the main mode of the surface AGW forcing to altitudes above 100 km, waves produce layers of convective instability and the peaks of the wave-induced jets at altitudes 100 – 120 km. Shorter AGWs with smaller horizontal wave speeds produce smaller mean heating and wave induced velocities in the upper atmosphere at the same amplitudes and periods of the surface wave excitation. Numerical simulation of nonlinear AGW propagation helps to better understanding the details of dynamical and thermal effects of waves coming from the troposphere on the mean temperature and wind in the middle and upper atmosphere.

Acknowlegements. This work was partly supported by the Russian Basic Research Foundation and by the Russian Science Foundation (grant 14-17-00685), and by the Ministry of Education and Science of Russian Federation (contract 3.1127.2014/K). The authors thank A. N. Gavrilov for help in improving computer code.

References.

Andreassen, O., Hvidsten, O., Fritts, D., Arendt, S. Vorticity dynamics in a breaking internal gravity wave. Part 1. Initial instability evolution. J. Fluid Mech. 367, 27–46, 1998

Baker, D., Schubert, G. Convectively generated internal gravity waves in the lower atmosphere of Venus. Part II: Mean wind shear and wavemean flow interaction. J. Atmos. Sci. 57, 200–215, 2000.

Clayson, C.A., Kantha, L. On turbulence and mixing in the free atmosphere inferred from high-resolution soundings, J. Atmos. Ocean. Technol., 25, 833–851, 2008

Djuth, F.T., Sulzer, M.P., Gonzales, S.A., Mathews, J.D., Elder, J.H., Walterscheid, R. L. A continuum of gravity waves in the Arecibo thermosphere. J. Geophys. Res. 31, L16801, doi:10.1029/2003GL019376, 2004.

Fritts, D.C., Garten, J.F. Wave braking and transition to turbulence in stratified shear flows. J. Atmos. Sci. 53 (8), 1057–1085, 1996.

Fritts, D.C., Alexander, M.J. Gravity wave dynamics and effects in the middle atmosphere. Rev. Geophys. 41(1), 1003, doi:10.1029/2001RG000106, 2003.

Fritts, D.C., Vadas, S.L., Wan, K., Werne, J.A. Mean and variable forcing of the middle atmosphere by gravity waves. J. Atmos. Solar-Terr. Phys. 68, 247–265, 2006.

Fritts, D.C., Wang, L., Werne, J., Lund, T., Wan, K. Gravity wave instability dynamics at high Reynolds numbers. Part II: turbulence evolution, structure, and anisotropy. J. Atmos. Sci. 66, 1149–1171, 2009

Fritts, D.C., Franke, P.M., Wan, K., Lund, T., Werne, J. Computation of clear-air radar backscatter from numerical simulations of turbulence: 2. Backscatter moments throughout the lifecycle of a Kelvin-Helmholtz instability. J. Geophys. Res. 116, D11105, doi:10.1029/2010JD014618, 2011.

Gavrilov, N.M. Structure of the mesoscale variability of the troposphere and stratosphere found from radio refraction measurements via CHAMP satellite. Izvestia, Atmos. Oceanic Phys. 43 (4), 451-460, 2007

Gavrilov, N.M. Estimates of turbulent diffusivities and energy dissipation rates from satellite measurements of spectra of stratospheric refractivity perturbations. Atmospheric Chemistry and Physics 13(23), 12107–12116, 2013.

Gavrilov, N.M., Fukao, S. A comparison of seasonal variations of gravity wave intensity observed by the MU radar with a theoretical model. J. Atmos. Sci. 56, 3485–3494, 1999.

Gavrilov, N.M., Luce, H., Crochet, M., Dalaudier, F., Fukao, S. Turbulence parameter estimations from high-resolution balloon temperature measurements of the MUTSI-2000 campaign . Annales Geophysicae 23, 2401-2413, 2005.

Gavrilov, N.M., Kshevetskii, S.P. Numerical modeling of propagation of breaking nonlinear acoustic-gravity waves from the lower to the upper atmosphere. Adv. Space Res., 51 (7), 1168–1174, doi:10.1016/j.asr.2012.10.023, 2013a.

Gavrilov, N.M., Kshevetskii, S.P. Study of acoustic-gravity wave propagation in the middle and upper atmosphere using numerical modeling. Chem. Phys. 32 (12), 65–72, (In Russian), 2013b.

Gavrilov, N.M., Kshevetskii, S.P. Numerical modeling of the propagation of nonlinear acoustic-gravity waves in the middle and upper atmosphere. Izvestiya, Atmos. Oceanic Phys. 50 (1), 66–72, 2014a.

Gavrilov, N.M., Kshevetskii, S.P. Verifications of the nonlinear numerical model and polarization relations of atmospheric acoustic-gravity waves. Geosci. Model Dev. Discuss. 7, 7805–7822, 2014b.

Gossard, E.E., Hooke, W.H. Waves in the atmosphere. Elsevier Sci. Publ. Co., Amsterdam-Oxford-New York, 1975.

Heale, C.J., Snively, J., Hickey, M.P., Ali C. Thermospheric dissipation of upward propagating gravity wave packets. J. Geophys. Res., 119 (5A),3857–387, doi:10.1002/2013JA019387, 2014.

Hedin, A.E. Neutral atmosphere empirical model from the surface to lower exosphere MSISE-90, Extension of the MSIS thermosphere model into the middle and lower atmosphere. J. Geophys. Res. 96, 1159—1172, 1991.

Karpov, I.V., Kshevetskii, S.P. Formation of large-scale disturbances in the upper atmosphere caused by acoustic gravity wave sources on the Earth's surface. Geomagn. Aeronomy 54 (4), 553–562, 2014.

Kshevetskii, S.P. Modelling of propagation of internal gravity waves in gases. Comput. Math. and Math. Phys. 41 (2), 295–310, 2001a.

Kshevetskii, S.P. Analytical and numerical investigation of nonlinear internal gravity waves. Nonlin. Proc. Geophys. 8. 37–53. 2001b.

Kshevetskii, S.P. Numerical simulation of nonlinear internal gravity waves. Comput. Math. and Math. Phys. 41 (12), 1777–1791, 2001c.

Kshevetskii, S.P., Gavrilov, N.M. Vertical propagation, breaking and effects of nonlinear gravity waves in the atmosphere. J. Atmos. Solar-Terr. Phys. 67(11), 1014–1030, doi: 10.1016/j.jastp.2005.02.013, 2005.

Larsen, M.F. A shear instability seeding mechanism for quasiperiodic radar echoes. J. Geophys. Res. 105, 24931–24940, 2000.

Larsen, M.F., Yamamoto, M., Fukao, S., Tsunoda, R.T., Saito, A. Observations of neutral winds, wind shears, and wave structure during a sporadic- E/QP event. Ann. Geophys. 23, 2369– 2375, doi:1432-0576/ag/2005-23-2369, 2005

Lax, P.D. Hyperbolic systems of conservation laws. Comm. Pure Appl. Math. 10, 537–566. 1957.

Lax, P.D., Wendroff, B. Hyperbolic systems of conservation laws. Comm. Pure Appl. Math. 13, 217–237. 1960.

Lindzen, R.S. Turbulence and stress owing to gravity wave and tidal breakdown, J. Geophys. Res. 86, 9707-9714, 1981.

Liu, H. -L. On the large wind shear and fast meridional transport above the mesopause. Geophys. Res. Lett. 34, L08815, doi:10.1029/2006GL028789, 2007.

Liu, X., Xu, J., Liu, H.-L., Ma, R. Nonlinear interactions between gravity waves with different wavelengths and diurnal tide. J. Geophys. Res. 113, D08112. doi:10.1029/2007JD009136, 2008.

Liu, X. , Xu, J., Gao, H., Chen, G. Kelvin-Helmholtz billows and their effects on mean state during gravity wave propagation. Ann. Geophys. 27, 2789-2798, 2009.

Liu, X., Xu, J., Yue, J., Vadas, S. L. Numerical modeling study of the momentum deposition of small amplitude gravity waves in the thermosphere. Ann. Geophys., 31, 1-14, doi:10.5194/angeo-31-1-2013, 2013.

Liu, X., Xu, J., Liu, H. -L., J. Yue, J., Yuan, W. Simulations of large winds and wind shears induced by gravity wave breaking in the mesosphere and lower thermosphere (MLT) region. Ann. Geophys. 32, 543-552, doi:10.5194/angeo-32-543-2014, 2014a.

Liu, X., Xu, J., Yue, J., Liu, H. –L., Yuan W. Large winds and wind shears caused by the nonlinear interactions between gravity waves and tidal backgrounds in the mesosphere and lower thermosphere. J. Geophys. Res. Space Phys., doi: 10.1002/2014JA020221, 2014b.

Lubken, F.-J. Rocket-borne measurements of small scale structures and turbulence in the upper atmosphere. Adv. Space Res. 17(11), 25–35, 1996.

MathWorks. Generalized bell-shaped membership function. http://www.mathworks.com/help/fuzzy/gbellmf.html. Accessed on December 2, 2014.

Medvedev, A.S., Gavrilov, N.M. The nonlinear mechanism of gravity wave generation by meteorological motions in the atmosphere. J. Atmos. Terr. Phys. 57, 1221–1231, 1995.

Park, J., L¨uhr, H., Lee, C., Kim, Y.H., Jee, G., Kim J.-H. A climatology of medium-scale gravity wave activity in the midlatitude/low-latitude daytime upper thermosphere as observed by CHAMP. J. Geophys. Res. Space Phys., 119, doi:10.1002/2013JA019705, 2014.

Richtmayer, R.R., Morton, K.W. Difference Methods for Initial-Value Problems. Intersci. Publ., New York. 1967.

Townsend, A.A. Excitation of internal waves by a turbulent boundary layer. J. Fluid. Mech. 22, 241–252, 1965.

Townsend, A.A. Internal waves produced by a convective layer. J. Fluid. Mech. 24, 307–319, 1966.

Vadas, S. L., Fritts, D. C. Thermospheric responses to gravity waves: Influences of increasing viscosity and thermal diffusivity. J. Geophys. Res. 110, D15103, doi:10.1029/ 2004JD005574, 2005.

Vadas, S. L., Nicolls M. J. The phases and amplitudes of gravity waves propagating and dissipating in the thermosphere: Theory. J. Geophys. Res. 117, A05322, doi:10.1029/2011JA017426, 2012.

Yiğit, E., Medvedev, A.S. Heating and cooling of the thermosphere by internal gravity waves, Geophys. Res. Lett. 36, L14807, doi: 10.1029/2009GL038507, 2009.

Yiğit, E., Medvedev, A. S. Internal gravity waves in the thermosphere during low and high solar activity: Simulation study. J. Geophys. Res. 115, A00G02, doi: 10.1029/2009JA015106, 2010.

Yiğit, E., Medvedev A. S. Gravity waves in the thermosphere during a sudden stratospheric warming. Geophys. Res. Lett. 39, L21101, doi:10.1029/2012GL053812, 2012.

Yiğit, E., Medvedev A. S. Internal wave coupling processes in Earth's atmosphere, Adv. Space Res., doi: 10.1016/j.asr.2014.11.020, 2014.

Yiğit, E., Aylward, A.D., Medvedev, A.S. Parameterization of the effects of vertically propagating gravity waves for thermosphere general circulation models: Sensitivity study. J. Geophys. Res. 113, D19106, doi:10.1029/2008JD010135, 2008.

Yiğit, E., Medvedev, A.S., Aylward, A.D., Hartogh, P., Harris, M.J. Modeling the effects of gravity wave momentum deposition on the general circulation above the turbopause. J. Geophys. Res. 114, D07101, doi:10.1029/2008JD011132, 2009.

Yiğit, E., Medvedev, A.S., Aylward, A.D., Ridley, A.J., Harris, M.J., Moldwin, M.B., Hartogh, P. Dynamical effects of internal gravity waves in the equinoctial thermosphere. J. Atmos. Sol.-Terr. Phys. doi:10.1016/j.jastp.2011.11.014, 2012a.

Yiğit, E., Ridley, A.J., Moldwin M.B. Importance of capturing heliospheric variability for studies of thermospheric vertical winds, J. Geophys. Res., 117, A07306, doi:10.1029/2012JA017596, 2012b.

Yiğit, E., Medvedev, A.S., England, S.L., Immel T.J. Simulated variability of the high-latitude thermosphere induced by small-scale gravity waves during a sudden stratospheric warming, J. Geophys. Res., 119, doi:doi:10.1002/2013JA019283, 2014.

Yu, Y., Hickey, M. P. Numerical modeling of a gravity wave packet ducted by the thermal structure of the atmosphere. J. Geophys. Res. 112, A06308, doi:10.1029/2006JA012092, 2007.

Yue, J., She, C. –J., Liu H. –L. Large wind shears and stabilities in the mesopause region observed by Na wind-temperature lidar at midlatitude. J. Geophys. Res., doi:10.1029/2009 JA014864, 2010.

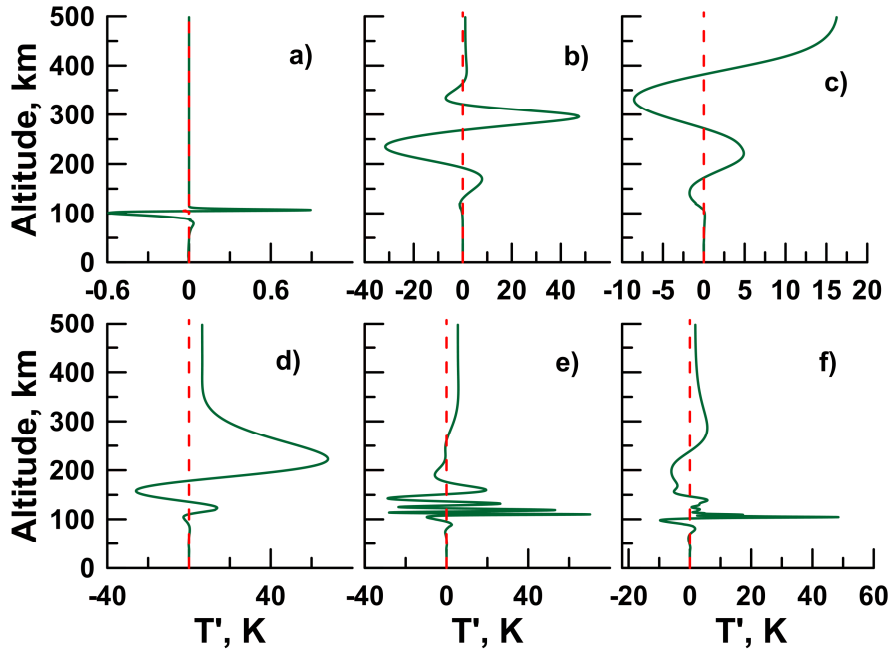

Figure 1. Vertical profiles of temperature perturbations produced by AGW source (5) with λ_h = 200 km and c_h = 100 m/s at fixed horizontal coordinate x = 3 km and at times t = 0.1 hr (a), 0.2 hr (b), 0.33 hr (c), 1 hr (d), 4 hr (e) and 8 hr (f).

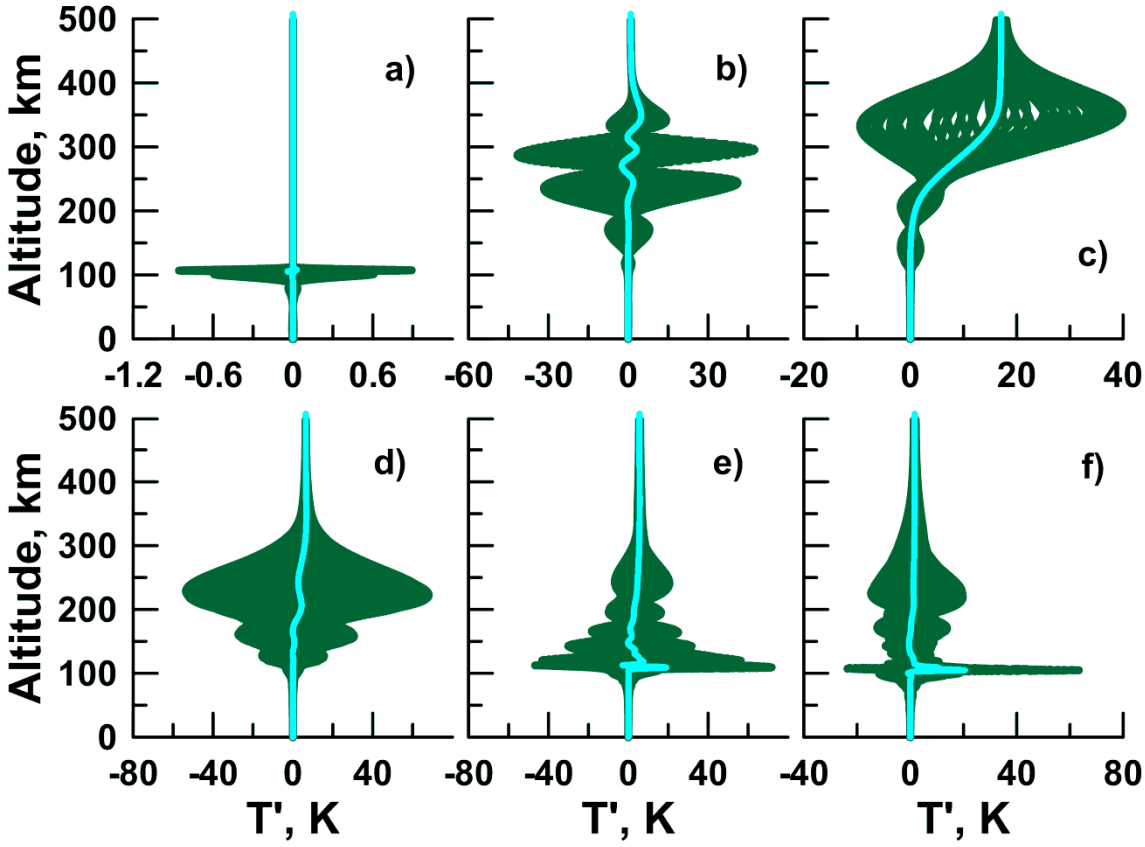

Figure 2. Vertical profiles of the ranges of temperature perturbations produced by AGW source (5) with λ_h = 200 km and c_h = 100 m/s at times t = 0.1 hr (a), 0.2 hr (b), 0.33 hr (c), 1 hr (d), 4 hr (e) and 8 hr (f). Thick lines show average values for each altitude.

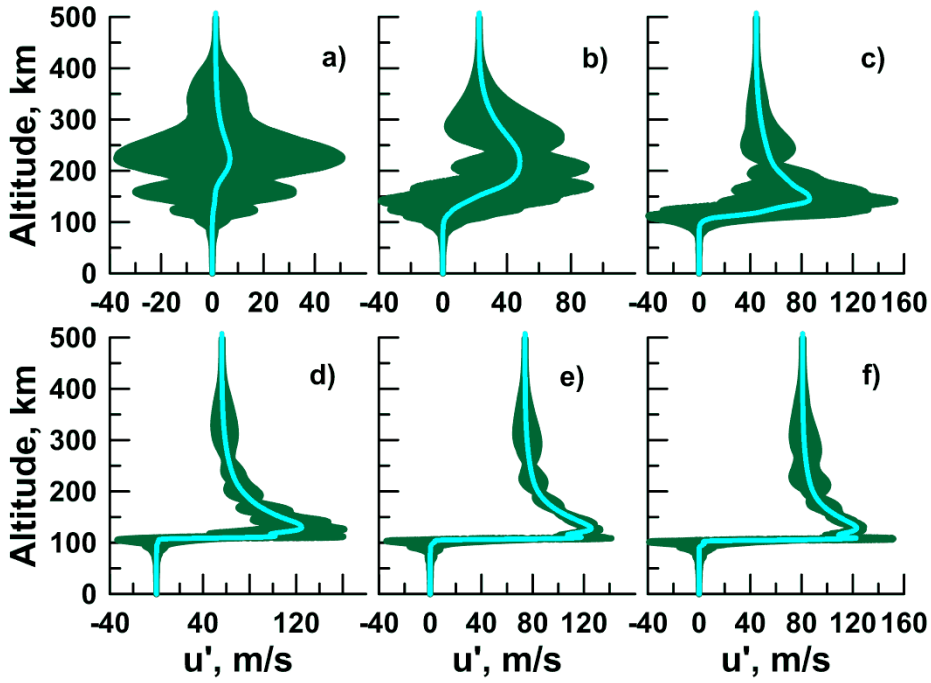

Figure 3. Vertical profiles of the ranges of horizontal velocity perturbations produced by AGW source (5) with λ_h = 200 km and c_h = 100 m/s at times t = 1 hr (a),2 hr (b), 3 hr (c), 4 hr (d), 6 hr (e) and 8 hr (f). Thick lines show average values for each altitude.

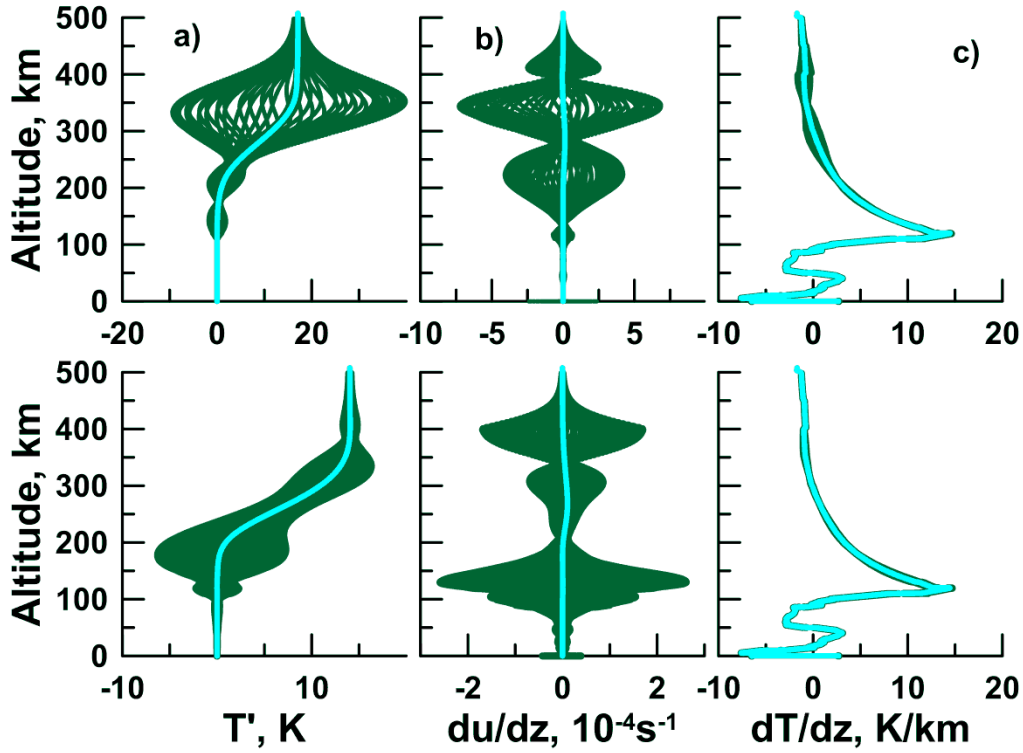

Figure 4. Vertical profiles of the ranges of temperature perturbations produced by AGW source (5) with λ_h = 200 km and c_h = 100 m/s (a), also respective vertical gradients of horizontal velocity (b) and temperature (c) at times t = 0.33 (top) and t = 0.5 hr (bottom). Thick lines show average values for each altitude.

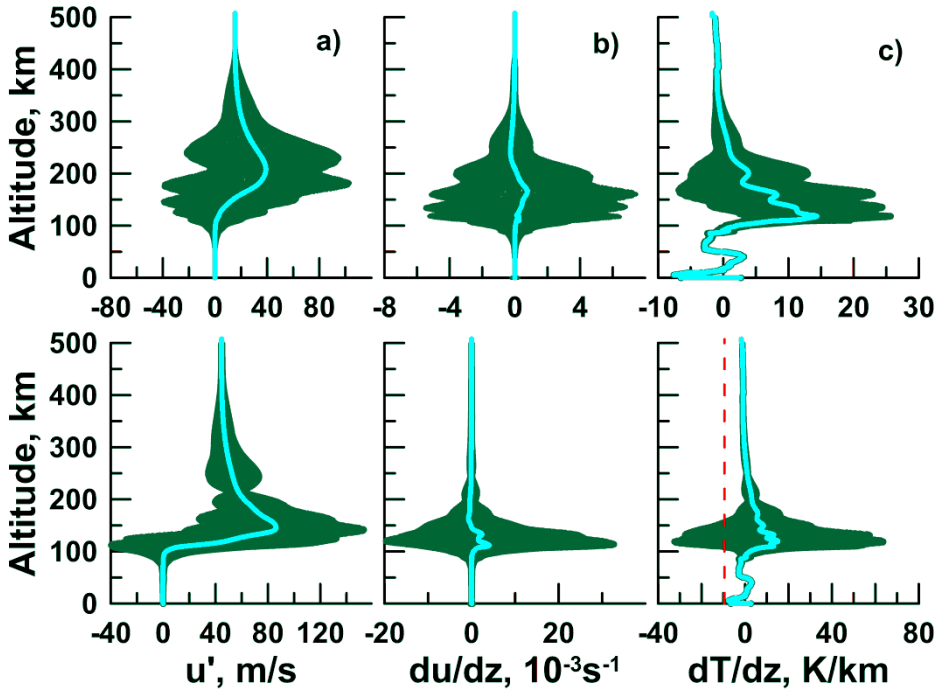

Figure 5. Vertical profiles of the ranges of horizontal velocity perturbations produced by AGW source (5) with λ_h = 200 km and c_h = 100 m/s (a), also respective vertical gradients of horizontal velocity (b) and temperature (c) at times t = 1.8 hr (top) and t = 3 hr (bottom). Thick lines show average values for each altitude. Dashed line shows adiabatic temperature gradient.

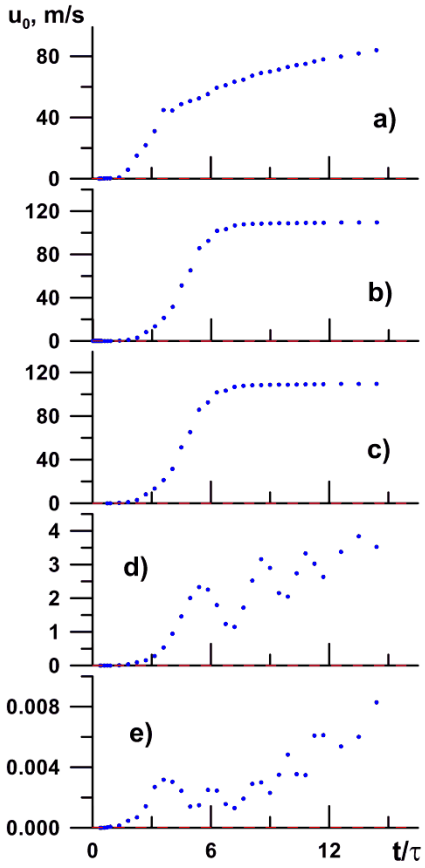

Figure 6. Time variations of the wave-induced mean horizontal velocity at altitudes z = 250 km (a), 150 km (b), 110 km (c), 100 km (d) and 60 km (e) for wave excitation with c_h = 100 m/s .

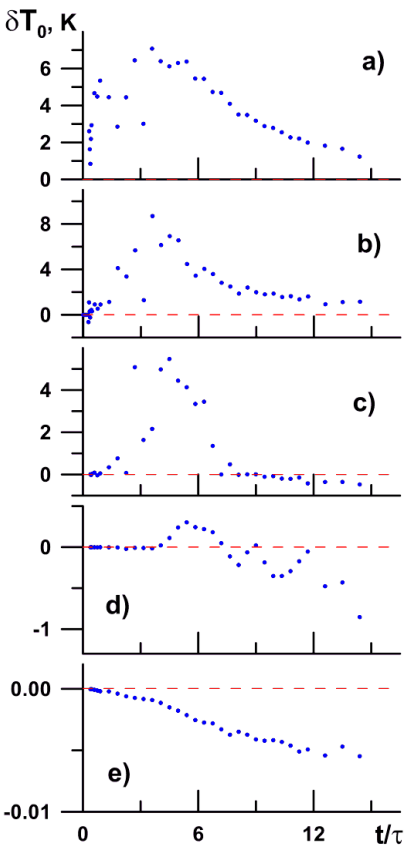

Figure 7. Same as Figure 6 but for changes in the mean temperature.

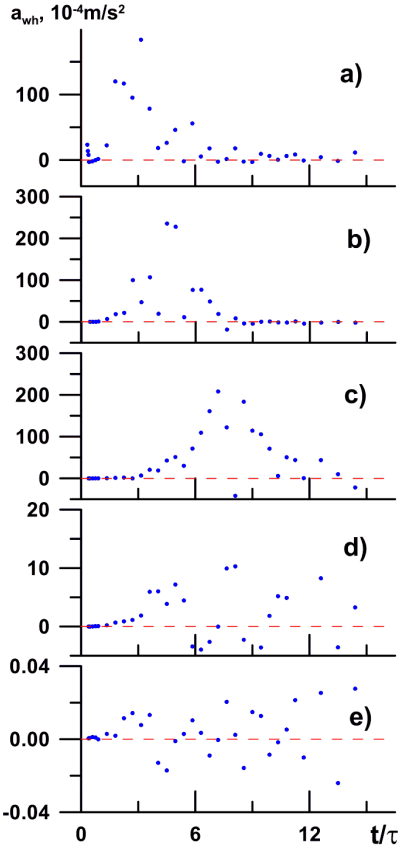

Figure 8. Time variations of horizontal wave drag at altitudes z = 250 km (a), 150 km (b), 110 km (c), 100 km (d) and 60 km (e).

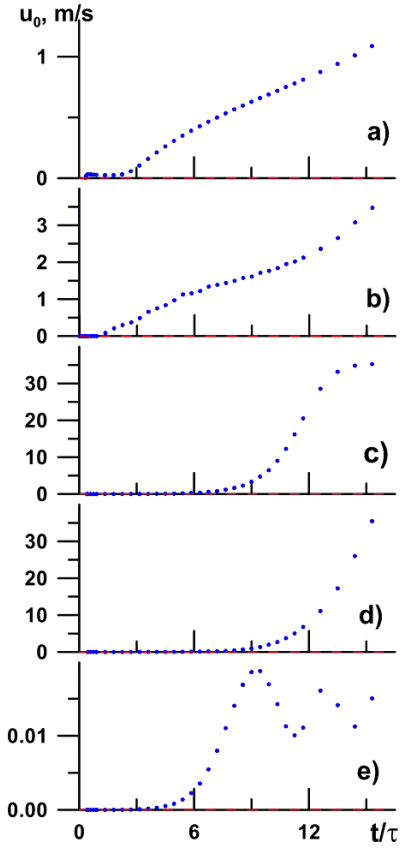

Figure 9. Same as Figure 6, but for the wave excitation with c_h = 30 m/s.

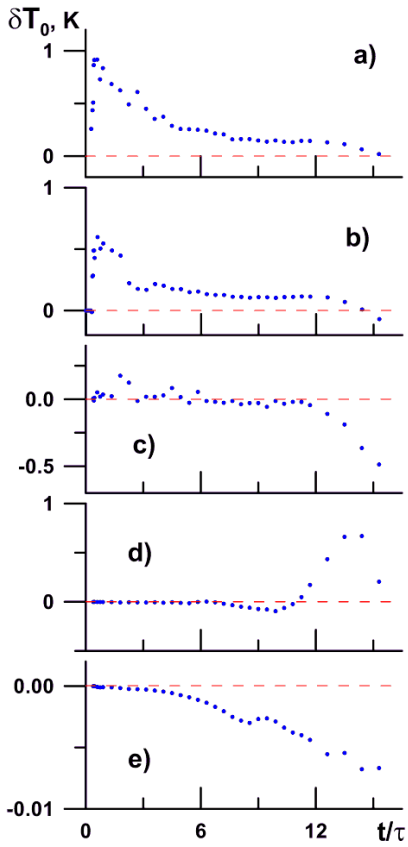

Figure 10. Same as Figure 7, but for the wave excitation with c_h = 30 m/s.